ACS APPLIED MATERIALS & INTERFACES

Research Article

www.acsami.org

Probing the Redox States at the Surface of Electroactive Nanoporous NiO Thin Films

Andrea G. Marrani,*[,†] Vittoria Novelli,[†] Stephen Sheehan,[‡] Denis P. Dowling,[‡] and Danilo Dini[†]

[†]Department of Chemistry, "Sapienza" University of Rome, Piazzale Aldo Moro 5, 00185 Rome, Italy

[‡]School of Mechanical and Materials Engineering, University College Dublin, Belfield, Dublin 4, Ireland

Supporting Information

ABSTRACT: Nanoporous NiO thin film electrodes were obtained via plasma-assisted microwave sintering and characterized by means of a combination of electrochemical techniques and X-ray photoelectron spectroscopy (XPS). The aim of this study is the elucidation of the nature of the surface changes introduced by the redox processes of this nanostructured material. NiO undergoes two distinct electrochemical processes of oxidation in aqueous electrolyte with the progress of NiO anodic polarization. These findings are consistent with the sequential formation of oxyhydroxide species at the surface, the chemical nature of which was assessed by XPS. Electronic relaxation effects in the Ni 2p spectra clearly indicated that the superficial oxyhydroxide species resulted to be β-NiOOH and γ-NiOOH. We also show for the first time spectral evidence of an electrochemically generated Ni(IV) species. This study has direct relevance for those applications in which NiO electrodes are utilized in aqueous electrolyte, namely catalytic water splitting or electrochromism, and may constitute a starting point for the comprehension of electronic phenomena at the NiO/organic electrolyte interface of cathodic dye-sensitized solar cells (p-DSCs).

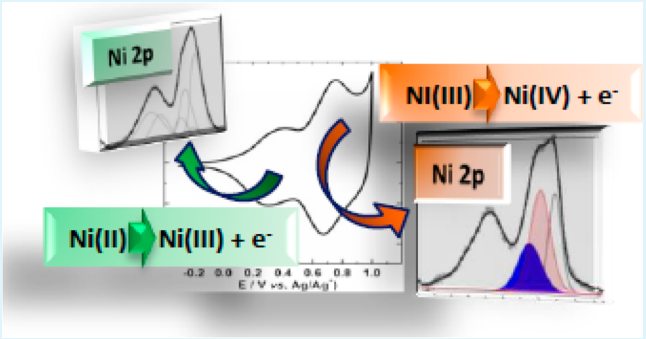

KEYWORDS: *nickel oxide, X-ray photoelectron spectroscopy, nanoporous electrode, cyclic voltammetry, dye-sensitized solar cell*

INTRODUCTION

Nickel oxide (NiO) presents p-type semiconducting features with the presence of a wide band gap (E_g > 3.50 eV) which can be modulated upon chemical and electrochemical doping.[1] Because of that, NiO is transparent in the visible spectrum when used in the configuration of a thin film with a thickness l < 3 μm.[2] The high chemical stability associated with its electrical/optical properties renders NiO a particularly intriguing material for those applications and technologies that require controllable changes of electrical conductivity and optoelectronic properties. In particular, NiO has been considered for energy storage applications,[3] electrochromic windows,[4,5] optoelectronic devices,[6] cathodic dye-sensitized solar cells (p-DSCs),[7−10] and, in more recent times, photoelectrochemical water splitting.[11,12]

The electronic structure of NiO has been long debated in the past[13] with no definitive understanding of its actual complexity. The most recent experimental results from electron spectroscopies provided a deeper insight into NiO electronic structure, taking advantage of the giant improvement of computational capabilities for the analysis of large sets of data. For a long time, NiO was considered a prototypical Mott−Hubbard insulator with an insulating gap caused by on-site Coulomb repulsion between 3d electrons, this energy gap being represented by the Hubbard U. In 1985, Zaanen, Sawatzky, and Allen proposed a new definition of NiO, in terms of electrical properties, as an intermediate compound between Mott−Hubbard insulators and charge-transfer (CT) semiconductors.[14] This is because they discovered that other states with a predominant ligand character fall inside the d−d correlation gap, thus leading to the formation of a much smaller CT gap (4.3 eV) between these states and the upper Hubbard d band.[15,16] NiO ground state can be described by the interaction among the $3d^8$, $3d^9\underline{L}$, and $3d^{10}\underline{L}^2$ configurations ($\underline{L}$ represents a hole in a ligand orbital),[15,17−20] where considerable electron transfer from the ligands to the central Ni atom occurs, leading to a Ni ground state charge of less than 2 in stoichiometric NiO.[21] The significant overlap between Ni 3d and O 2p orbitals in NiO gives rise to complex XP spectra, especially in the region of Ni 2p photoionization. The photoemission-induced formation of a core-hole in the Ni atom, $d^8 \rightarrow \underline{c}d^8$ (where $\underline{c}$ denotes a hole in the 2p level), is accompanied by a screening mechanism where electrons are transferred to the Ni site from the neighboring ligands. Therefore, in the final core-hole ionized state the lowest energy is of $\underline{c}d^9\underline{L}$ character, followed by the doubly screened $\underline{c}d^{10}\underline{L}^2$ and unscreened $\underline{c}d^8$ states.[22,23] A matter of long debate has been the interpretation of a shoulder signal in the Ni $2p_{3/2}$ XP spectrum located at ∼1.5 eV at the high binding

Received: August 29, 2013
Accepted: December 10, 2013
Published: December 10, 2013

 © 2013 American Chemical Society

energy side of the $\underline{c}d^9\underline{L}$ main feature. Many hypotheses were proposed during the years to explain the nature of such peak, as the one which assigns it to Ni^{3+} ions,[24−27] their presence being associated with an increased defectiveness of the crystal upon repeated Ar^+ sputtering cycles.[28] This explanation was rejected, since it is well known that Ar^+ bombardment preferentially leads to O vacancies, with the consequent reduction of the valency of Ni centers.[29,30] Controversies also arose in the past to decide whether the final state configuration of the shoulder was $\underline{c}d^9\underline{L}^2$, hence tightly associated to defective Ni^{3+} sites[27] or $\underline{c}d^{10}\underline{L}^2$.[31,32] A further contradiction to its attribution to Ni^{3+} defects came from X-ray absorption spectroscopy (XAS) studies, which demonstrated that extra holes in NiO reside primarily on O ligands and show a strong antiferromagnetic coupling with the Ni spin state.[22,33] A new light was shed on the plethora of attributions proposed until then, when Van Veenendaal and Sawatzky[34] extended the size of the cluster used for the calculations to Ni_7O_{36}, adopting a multisite cluster approach which included the contributions from nearest neighbor Ni sites. On a theoretical basis, they could justify the presence of the above mentioned shoulder in the Ni 2p XP spectrum as due to a *nonlocal screening* effect, wherein a hole is transferred from a ligand of the core-ionized site to the ligands of a nearest neighbor cluster, according to the general process $\underline{c}d^{n+1}\underline{L}:d^n \rightarrow \underline{c}d^{n+1}:d^n\underline{L}$, where the ":" symbol denotes two adjacent clusters. This theory was able to correctly explain the experimental XP spectra of various NiO-based systems, such as $Ni_xMg_{1-x}O$[35−37] and epitaxially grown NiO monolayers on MgO,[23] where the high dilution of NiO_6 (impurity-like) clusters into the host oxide matrix (or surface) caused the disappearance of the nonlocal screening induced final state. The surface sensitivity of the shoulder intensity has been reported many times after the first evidences discussed in ref 23 as, for example, in the case of nanostructured systems (e.g. nanoislands and nanoparticles)[38−42] with a larger surface-to-volume ratio compared to flat crystalline NiO (100) surfaces. In this case, the shoulder intensity was shown to increase significantly. In the frame of the nonlocal screening interpretation, such surface effects have recently been reconsidered[38,39,43] by applying configuration interaction (CI) calculations to a NiO_5 cluster with a pyramidal coordination symmetry coupled to a NiO_6 cluster. The calculations on such a lower symmetry double cluster generated two spectral contributions, which adequately reproduce the experimental intensity of the shoulder signal and account for the structural and chemical properties of NiO-based materials.

As to the other nickel oxides and hydroxides, their photoemission signatures were studied in the work of Grosvenor et al.[44] using the intra-atomic multiplet structures calculated by Gupta and Sen (GS)[45,46] for free transition-metal ions.

In the present work, we have considered the scalable method of plasma-assisted microwave sintering[7] for the preparation of nanoporous NiO electrodes intended for photoelectrochemical applications requiring cathodes of high surface areas.[7−12] In particular, we have deposited NiO thin films ($0.2 < l < 3.5$ μm) by spraying films of NiO nanoparticles (diameter $\approx$ 50 nm) onto fluorine-doped tin oxide (FTO)/glass substrates, and successively, we have conducted the step of sintering with the microwave radiation. This deposition technique has proved to be successful in the preparation of efficient NiO photoactive coatings for *p*-DSCs,[47] with the display of good mechanical stability, strong adhesion of the oxide film on technical substrates, and excellent photoelectrochemical properties.[7] The synthesized NiO obtained via microwave sintering has been characterized in the configuration of thin film electrodes ($0.2 < l < 3.5$ μm) by coupling a truly surface-sensitive technique, such as X-ray photoelectron spectroscopy (XPS), with electrochemical methods. The aim of the work is the elucidation of the nature of the surface changes that accompany the electrochemical processes of the nanoporous electrodes here considered by studying the electronic relaxation effects in the core levels (Ni 2p and O 1s) of NiO. The use of aqueous electrolyte is here intended as the optimal condition to put in evidence the changes in oxidation state, possibly leading to formation of different Ni compounds, occurring when a NiO nanoporous thin film undergoes high potential polarization. It is, therefore, to be considered as a preliminary screening of the possible behavior of NiO when used as a cathode in *p*-DSCs equipped with either all-organic or water-contaminated organic electrolytes.

EXPERIMENTAL SECTION

NiO Coating Deposition. NiO nanoparticles with diameter 50 nm (99.8 % grade from Sigma-Aldrich) were suspended in methanol at the concentration of 20 mg mL^{-1}. The resulting slurry was spray-deposited onto fluorine-doped tin oxide (FTO)-coated glass (12 Ω/sq, 3 mm thick, from Sigma-Aldrich), using a technique similar to that reported in a previous work.[48] The area of the NiO samples was 5 mm × 5 mm. The cleaning of the FTO-coated glass substrates (area: 2 cm × 2 cm) was carried out for a total of 45 mins: 15 mins in soapy deionized water, 15 mins in 2-propanol, and 15 mins in acetone (all in ultrasonic bath). The range of NiO thickness which has been encompassed in the present work is 0.2−3.5 μm. The minimum film thickness of 0.2 μm was obtained with a single pass of spraying whereas largest thicknesses require multiple passes of spraying. Every NiO sample was treated with microwave radiation (vide infra) in a single step after the completion of spray deposition. The sintering of the spray-deposit was effectuated with plasma-assisted microwave heating using the experimental setup described in detail in ref 49. Such a procedure of deposition is also known as rapid discharge sintering (RDS).[47−49] In the adopted experimental conditions plasma could be formed at the total pressure of 5 mbar in an Ar/O_2 atmosphere with volume ratio $Ar:O_2$ = 10:1 when an input power of 2.4 kW was used. The microwave power supply (from Mugge) operated at the frequency of 2.45 GHz. The temperature of sintering was about 450 °C while the treatment time was 5 mins.[13]

NiO Characterization. The thickness of the NiO films was evaluated by step height measurement using a WYKO NT1100 optical profilometer in the vertical scanning interferometry (VSI) mode. For morphology analysis, the samples were examined using a FEI Quanta 3D FEG DaulBeam system (FEI Ltd, Hillsboro, USA). The resulting NiO films obtained with plasma-assisted sintering displayed nanoporous features as visualized in the SEM picture of sample cross-section (Figure 1).

The redox properties of NiO electrodes were studied using a custom-made cell with a three-electrode configuration: NiO-covered FTO was the working electrode, a Pt wire was the counter electrode, and Ag/AgCl (KCl 3 M, E vs NHE = 0.210 V) was used as reference electrode. The electrolyte was 0.2 M KCl, 0.01 M KH_2PO_4, 0.01 M Na_2HPO_4 in H_2O. The applied potential values were referred to the Ag/AgCl reference electrode. Cyclic voltammetries were determined with the potentiostat/galvanostat Autolab PGSTAT 128 N and recorded with the NOVA 1.9 software.

XPS measurements were performed using a modified Omicron NanoTechnology MXPS system equipped with a monochromatic X-ray anode (Omicron XM-1000), a dual X-ray anode (Omicron DAR 400), and an Omicron EA-127 7-channeltron energy analyzer. The experimental conditions adopted were the following: excitation by Al Kα photons ($h\nu$ = 1486.7 eV, monochromatic X-ray anode) and Mg

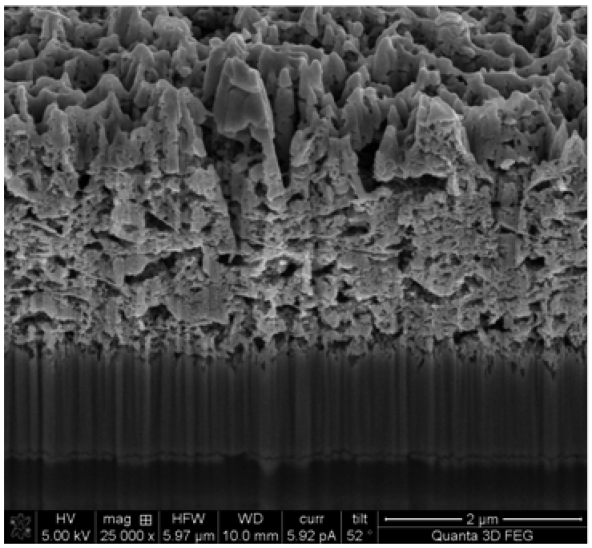

Figure 1. SEM cross-sectional view of a NiO film sintered via plasma-assisted microwave heating ($2 < l < 3$ μm).

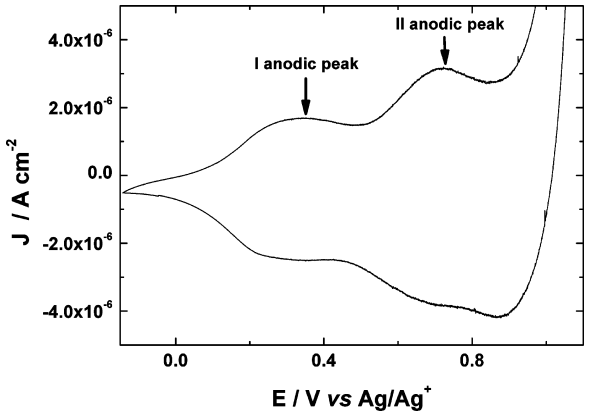

Figure 2. Cyclic voltammogram of NiO (thickness: 0.2 μm, NiO nanoparticles diameter: 50 nm). Scan rate: 2 mV s^{-1}; electrolyte: 0.2 M KCl, 0.01 M KH_2PO_4, 0.01 M Na_2HPO_4 in H_2O.

Kα photons ($h\nu$ = 1253.6 eV, dual X-ray anode), both generated operating the anode at 14 kV, 16 mA. The monochromatic X-ray source was used in order to gain the maximum resolution power and to discern the numerous spectral features in the Ni 2p region of bulk NiO. The non-monochromatic Mg Kα source was utilized to achieve a higher sensitivity towards the surface species at the same take-off angles (θ) with respect to the former source. No charging was experienced during measurements. For all the samples, the regions associated to ionization of Ni 2p, O 1s, and C 1s levels and to the $L_{2,3}M_{4,5}M_{4,5}$ Auger transition were acquired using an analyzer pass energy of 20 eV, while a survey scan was also taken at 50 eV pass energy. Take-off angles of 11° and 83° with respect to the sample surface normal were adopted. The measurements were performed at room temperature and the base pressure in the analyzer chamber was about 2×10^{-9} mbar during the spectra detection. The binding energy (BE) of the C 1s line at 284.8 eV, associated to adventitious carbon species, was used as an internal standard reference for BE scale (accuracy of ±0.1 eV). The experimental spectra were theoretically reconstructed by fitting the secondary electrons background to a Shirley function and the elastic peaks to symmetric Voigt functions described by a common set of parameters (position, FWHM, Gaussian–Lorentzian ratio) free to vary within narrow limits. The Gaussian–Lorentzian ratio varied between 0.8 and 0.9. The Shirley background was drawn over the entire Ni 2p envelope, roughly in the range between 848 and 888 eV BE applying a small offset at the high BE end point, in order to better reproduce the separation between the $2p_{3/2}$ and $2p_{1/2}$ spectral portions.[50] After fitting, the optimized background was subtracted from the experimental spectrum. XPS atomic ratios between relevant fitting components of the same orbital region were estimated from experimentally determined area ratios (±10% associated error). Depth of analysis (d) was determined according to the formula $d = 3\lambda(\mathrm{KE}) \cos\theta$, where θ is the take-off angle and λ(KE) is the inelastic mean free path (IMFP) of electrons escaping the surface with a kinetic energy KE. The IMFP values were calculated using the NIST Electron Inelastic-Mean-Free-Path Database[51] with the TPP-2M equation.[52] The d values found for Ni 2p and O 1s electrons as a function of θ and X-ray source used are reported in Table S1 (see the Supporting Information (SI)).

RESULTS AND DISCUSSION

Electrochemistry. The cyclic voltammogram of microwave sintered NiO in aqueous electrolyte presents two characteristic broad oxidation waves with reversible features (Figure 2). The first of the two waves of current, i.e. the one at the lowest potential (oxidation peak I), is generally attributed to the transformation of Ni(II) into Ni(III) in the oxide (eq 1):[53,54]

$$\mathrm{NiO(OH)}_n(\mathrm{H_2O})_p \rightarrow \mathrm{NiO(OH)}_{n+1}(\mathrm{H_2O})_{p-1} + e^- + \mathrm{H^+} \quad (1)$$

For the second wave of current at the highest potential (oxidation peak II), there is still ambiguity for the assignment of the redox process, since either the oxidation Ni(II) → Ni(III) (as written in eq 2) or the oxidation Ni(III) → Ni(IV) (as written in eqs 3a and 3b) can originate the signal at about 0.7 V vs Ag/AgCl (Figure 2), depending on the extent of hydration of the metal oxide.[55−57]

$$\mathrm{NiO(OH)}_m \rightarrow \mathrm{NiOO(OH)}_{m-1} + e^- + \mathrm{H^+} \quad (2)$$

$$\mathrm{NiO(OH)}_{n+1}(\mathrm{H_2O})_{p-1} \rightarrow \mathrm{NiO(OH)}_{n+2}(\mathrm{H_2O})_{p-2} + e^- + \mathrm{H^+} \quad (3a)$$

$$\mathrm{NiOO(OH)}_{m-1} \rightarrow \mathrm{NiO_2(OH)}_{m-2} + e^- + \mathrm{H^+} \quad (3b)$$

The first oxidation peak appears slightly broader than the second one, probably because of the variability of the acidity of the water molecules coordinated by the Ni(II) centers on the surface (eq 1). Such a variability is expected to be associated with a distorted and irregular geometry of coordination by the surface Ni centers. Upon cycling this peak tends to diminish its height quite rapidly, mainly because of the progressive replacement of surface water with hydroxyl groups (Figures S1 (SI) and 5). This has been partially confirmed by the relative decrease of the height of the first peak compared to the second oxidation peak when plasma sintered NiO samples undergo a thermal treatment at 300 °C prior to the electrochemical cycling in aqueous electrolyte (not shown). When the charge compensating process of NiO oxidation is represented by the removal of a proton from an hydroxyl group coordinated by surface Ni centers (eqs 2 and 3b, oxidation peak II), the peak appears sharper (Figures 2 and S2 (SI)), probably because of a more regular coordination geometry of hydroxyl-coordinating surface Ni sites with valence >2. Figure 3a shows the voltammograms of NiO in aqueous electrolyte recorded at different scan rates. Each voltammogram was recorded on a freshly prepared NiO sample; therefore, ruling out possible degradation effects of NiO in the aqueous electrolyte (vide infra). The dependence of the oxidation and reduction peaks of

dx.doi.org/10.1021/am403671h | ACS Appl. Mater. Interfaces 2014, 6, 143−152

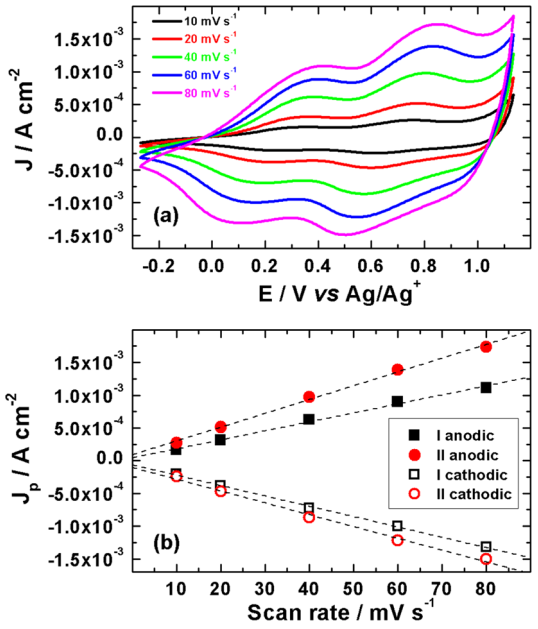

Figure 3. (a) Cyclic voltammograms of NiO (thickness: 1.1 μm) at five different scan rates, ranging from 10 to 80 mV s^{-1}. Fresh NiO samples were utilized at each scan rate. (b) Linear dependence of anodic and cathodic peak currents (J_p) with the scan rate for both first (I) and second (II) redox reactions at the surface of NiO (data extracted from part a). Electrolyte: 0.2 M KCl, 0.01 M KH_2PO_4, 0.01 M Na_2HPO_4 in H_2O. NiO samples prepared as in Figure 2.

nanoporous NiO is generally linear with the scan rate (Figure 3b).[47,55] This behavior indicates that the redox reactions of the nanoporous NiO samples here considered are kinetically controlled by a charge transfer process confined at the NiO–electrolyte interface.[48] Therefore, the NiO obtained via RDS of oxide nanoparticles displays the same type of electrochemical behavior of nanostructured NiO prepared via a sol–gel route.[55]

When the voltammograms of nanoporous NiO films having different thicknesses are compared (Figure 4), the direct proportionality between the intensity of the current density peaks (J_p) and the thickness of the NiO films can be observed. These findings are indicative of the electroactivity of nanoporous NiO film throughout the whole thickness and of the

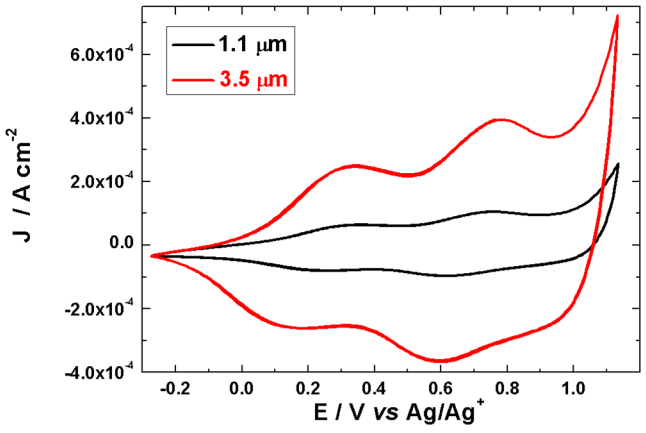

Figure 4. Cyclic voltammograms of NiO samples with two different thicknesses at the scan rate 10 mV s^{-1}. Electrolyte: 0.2 M KCl, 0.01 M KH_2PO_4, 0.01 M Na_2HPO_4 in H_2O. NiO samples prepared as in Figure 2.

effectiveness of the electrical contact at the NiO/FTO interface.[47,58] The continuous cycling of nanoporous NiO in aqueous electrolyte has a deleterious effect on the oxide with the progressive disappearance of the two characteristic oxidation peaks (Figure 5a) and the flattening of the voltammogram after about a hundred of cycles (Figure 5b).

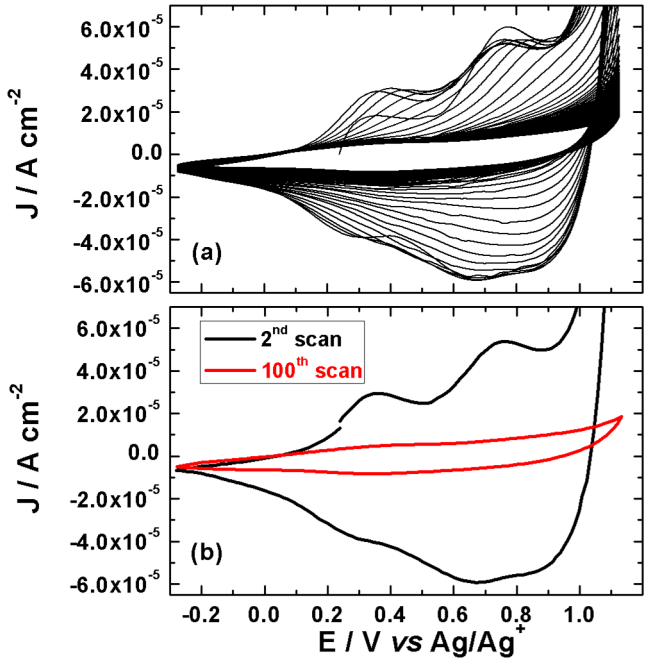

Figure 5. Effect of repetitive cycling on NiO voltammograms. (a) Whole set of 100 cycles. (b) Comparison between the 2nd and the 100th cycle. NiO thickness: 1.1 μm; scan rate: 5 mV s^{-1}. Electrolyte: 0.2 M KCl, 0.01 M KH_2PO_4, 0.01 M Na_2HPO_4 in H_2O.

The dissolution of the metal oxide/hydroxide interface is at the basis of this observation, and is induced by the prolonged contact of the oxide with the aqueous electrolyte. NiO dissolution is favored also by the process of oxidation itself since this brings about an increase of surface polarity, producing significant tensile stresses compared to the pristine oxide.[59] As a consequence of that, the electromechanical tensions associated with the increase of charge density at the surface of the oxidized coating are relieved through the partial dissolution of the oxidized film.

Prior to the recording of the X-ray photoelectron spectra (vide infra), the NiO samples with thickness 2.5 μm were polarized for 1000 s at two values of applied potential, namely 0.5 and 0.85 V vs Ag/AgCl, which correspond to the two distinct oxidized states of NiO (Figure S1 in the SI). In order to minimize exposure to ambient contaminants and avoid possible degradation issues, such polarized samples, henceforth respectively referred to as NiO0.5 and NiO0.85, were introduced in the XPS chamber within the least possible time after polarization (1–2 min). For the sake of comparison, XPS data were recorded also for the as-prepared NiO reference sample with the same thickness value (simply referred to as NiO in the forthcoming figures).

XPS. In order to record a spectroscopic signal for the bulk of NiO to be used as a reference for the interpretation of all other spectra, the Al Kα X-ray monochromatic source was used in the bulk-sensitive (θ = 11°) mode to collect spectra of the NiO samples just after deposition, without any further treatment.

dx.doi.org/10.1021/am403671h | ACS Appl. Mater. Interfaces 2014, 6, 143–152

Nevertheless, for an optimal assessment of surface-related phenomena, all the commented spectra, except those in Figures 6 and 7, were acquired using a less energetic photon source, the

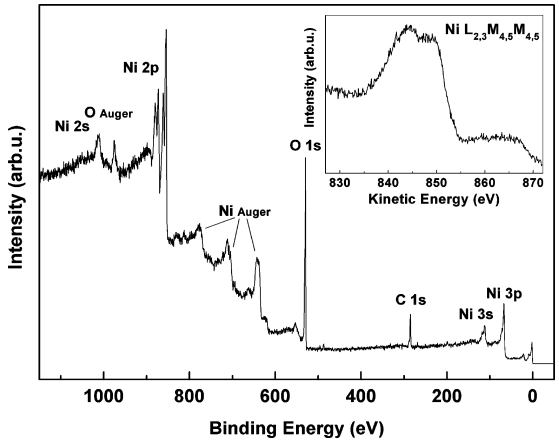

Figure 6. Survey XP spectrum and Ni $L_{2,3}M_{4,5}M_{4,5}$ Auger transition (inset) of NiO sample recorded at θ = 11° with the Al Kα X-ray monochromatic source.

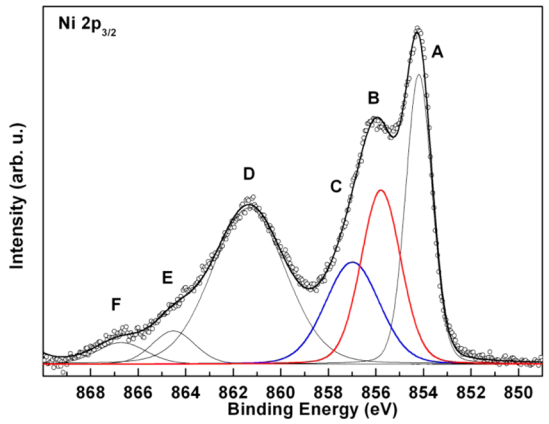

Figure 7. Ni $2p_{3/2}$ XP experimental (dots) spectrum of NiO sample recorded at θ = 11° take-off angle with Al Kα X-ray monochromatic source, and fitting reconstruction (line). Single components marked with capital letters (A–F) are referred to in the text. Components B and C are evidenced in red and blue colors, respectively.

X-ray Mg Kα anode ($h\nu$ = 1253.6 eV), in the most surface-sensitive mode available, namely at θ = 83°, which provided a shorter IMFP of Ni 2p photoelectrons (see Figure S5 in the SI for a comparison between Ni $2p_{3/2}$ spectra of reference NiO sample taken with Al Kα and Mg Kα at θ = 73°).

The survey XP spectrum of the reference NiO sample is reported in Figure 6, together with the Ni $L_{2,3}M_{4,5}M_{4,5}$ Auger transition (inset, see the SI for discussion). The survey spectrum shows the signals associated to Ni and O, and a small contribution from C due to contamination from environment or from pump oil inside the UHV chamber, while the shape and the position of Auger signals are compatible with literature data on NiO (see the SI).[17]

Ni 2p. The 3/2 spin-orbit component of Ni 2p ionization region is reported in Figure 7 for the reference NiO sample (for overall Ni 2p region, see Figure S6 in the SI). The experimental signal has been reconstructed by fitting to six different Voigt peaks with a Gaussian/Lorentzian (G/L) ratio of 0.85 (i.e. 85% Gaussian shape contribution), the BE position and full-width at half-maximum (FWHM) values being reported in Table 1. Such peaks have been called for simplicity A, B, C, D, E, and F

Table 1. Binding Energy Position (BE) and FWHM Values of Peaks Used in the Fitting of the Ni $2p_{3/2}$ Spectrum of As-Prepared Nanoporous NiO[a]

peak	cluster model final state configuration	BE (eV)	FWHM (eV)
A	$\underline{c}d^9\underline{L}$	853.7	1.31
B	d^8:$\underline{c}d^9\underline{L}$[b]	855.3	1.97
C	$\underline{c}d^9$:d^7[c]	856.5	2.68
D	$\underline{c}d^{10}\underline{L}^2$	860.8	3.64
E	$\underline{c}d^8$	864.0	2.11
F	shake-up	866.2	2.46

[a]Spectrum was acquired with monochromatic Al Kα source at θ = 11° take-off angle. [b]For a NiO_6:NiO_5 cluster, on-site screening of a NiO_5 Ni 2p core-hole (see ref 43). [c]For a NiO_6:NiO_5 cluster, inter-site screening of a NiO_6 Ni 2p core-hole (see ref 43).

in the order of increasing BE, and they have been assigned to different electronic configurations in the final state after the creation of the 2p core-hole upon photoemission. The lowest BE feature at 853.7 eV (peak A) and those at 860.8 eV (peak D) and 864.0 eV (peak E) are unanimously attributed to the $\underline{c}d^9\underline{L}$, $\underline{c}d^{10}\underline{L}^2$, and $\underline{c}d^8$ states,[22,23] respectively.

These states originate from an on-site CT process between the ligand anions and the central Ni cation, with the latter representing the locus where the core-hole resides. The highest BE feature in the $2p_{3/2}$ envelope at 866.2 eV (peak F) is attributed to shake-up transitions.[44,50] The relative positions of the so far mentioned peaks are fully consistent with literature data on similar systems.[44,50]

The signals at 855.3 eV (peak B) and 856.5 eV (peak C) are here attributed to an inter-site CT screening process where both the *non-local* (peak C) and the *surface-sensitive* (peak B) components are present. These two peaks were introduced in the simulation of the experimental Ni $2p_{3/2}$ spectra of the present work on the basis of the CI calculations reported by Soriano et al. on a NiO_6:NiO_5 double cluster.[38,39,43] These authors reported that the shoulder at the high-BE side of the double-peaked main structure of Ni $2p_{3/2}$ spectrum can reasonably be fit to two components representing the d^8:$\underline{c}d^9\underline{L}$ state, where the core-hole is formed in the NiO_5 unit followed by on-site CT screening and the already known nonlocal screening contribution peak. The NiO_5 unit is thus representative of a *surface* environment, where the coordination symmetry of Ni ions is lowered, and its contribution to the Ni 2p spectrum can be reproduced by peak B. As to the nonlocal screening contribution, its final state configuration slightly differs from the seminal paper by Van Veenendaal et al.,[34] in which they reported it as a $\underline{c}d^9$:$d^8\underline{L}$ state of two adjacent NiO_6 units in a Ni_7O_{36} cluster, whereas Soriano et al.[38,43] attributed it to a $\underline{c}d^9$:d^7 state of the NiO_6:NiO_5 cluster (see the SI for further comments). In the lack of a complete ab initio calculation describing the Ni 2p spectrum, in this work we have simulated the XP Ni $2p_{3/2}$ regions in the 854–858 eV energy range of all the commented NiO samples using the nonlocal screening approach in the version implemented in ref 43. The simulation of the Ni $2p_{3/2}$ XP spectrum of the reference NiO sample performed using the six components above described satisfactorily reproduces the experimental line shape (Figure 7).

In Figure 8, the experimental Ni $2p_{3/2}$ XP spectra of (a) NiO (reference), (b) NiO0.5, and (c) NiO0.85 samples are reported

dx.doi.org/10.1021/am403671h | ACS Appl. Mater. Interfaces 2014, 6, 143–152

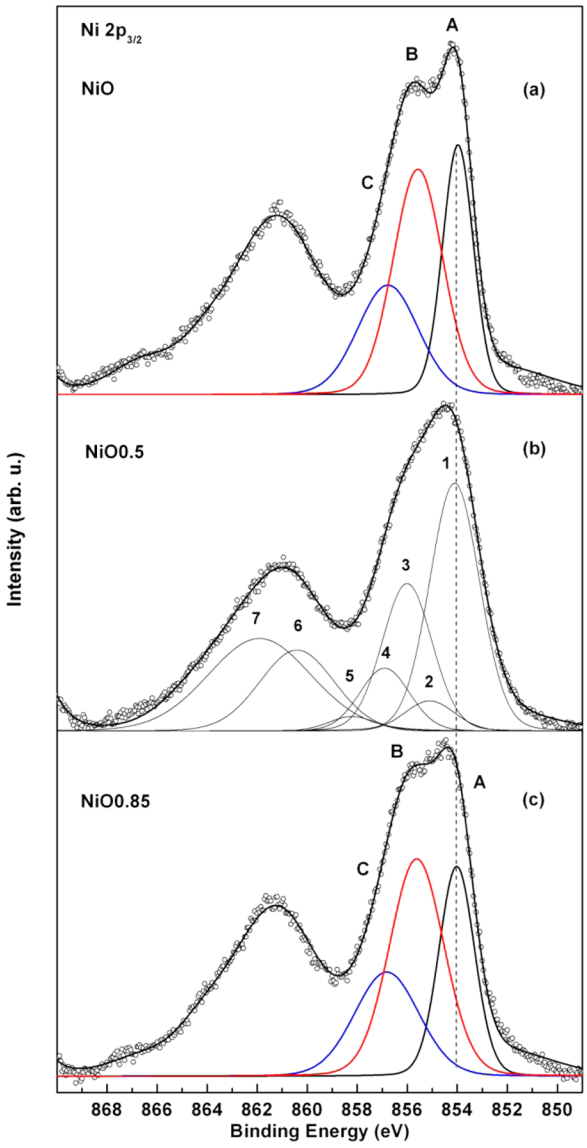

Figure 8. Ni $2p_{3/2}$ XP experimental (dots) spectra of (a) NiO, (b) NiO0.5, and (c) NiO0.85 samples recorded at take-off angle θ = 83° with Mg Kα X-ray source and fitting reconstruction (line) with relevant single components [A–C in spectra a and c, and 1–7 in spectrum b].

together with the fitting reconstruction results, namely the convoluted envelope of peaks and the relevant single components. The BE positions and FWHM values of the latter are reported in Tables 2 and 3.

In the case of the as-prepared NiO sample, here taken as reference, only the first three components (peaks A, B, and C) are reported for the sake of clarity, since their intensities are the

Table 2. Binding Energies (eV)/ FWHM (eV) Values of Peaks A, B, and C Used in the Fitting of Ni $2p_{3/2}$ Spectra of NiO and NiO0.85 Samples[a]

sample	peak A	peak B	peak C
NiO	854.0/1.45	855.6/2.33	856.8/2.85
NiO0.85	854.0/1.68	855.6/2.56	856.8/3.03

[a]Spectra were acquired using Mg Kα photons at a θ = 83° take-off angle.

Table 3. BE and FWHM Values of Peaks Used in the Fitting of Ni $2p_{3/2}$ Spectrum of Sample NiO0.5[a]

peak	BE (eV)[b]	FWHM (eV)
1	854.1	2.35
2	855.1	2.35
3	856.0	2.35
4	856.9	2.35
5	858.2	2.19
6	860.4	3.53
7	861.9	4.86

[a]Spectrum was acquired using Mg Kα photons at θ = 83° take-off angle. [b]BE relative values according to ref 44.

most affected by surface effects. The main difference between spectrum a of Figure 8 and that already discussed in Figure 7 is the intensity of peak B relative to peaks A and C. According to the data reported in Table S1 (see the SI), a depth (d) of 0.35 nm is investigated in spectrum a of Figure 8 compared to the depth of 3.8 nm analyzed in the spectrum of Figure 7. This difference in d leads to a sizeable variation in the ratios of the areas of peaks A, B, and C, increasing for the B/A ratio from 0.90 (Figure 7) to 1.45 of spectrum a (Figure 8). Such important variation has to be ascribed to the intrinsic superficial nature of the $\underline{c}d^9\underline{L}$ final state represented by peak B, wherein the core-hole belonging to a lowered symmetry NiO_5 unit[43] is reasonably expected to be confined at the surface. The ratio C/A also increases from 0.72 to 0.86 in the same sequence, since the higher concentration of NiO_5 units at the surface increases the contribution of nonlocally screened $\underline{c}d^9:d^{7}$[43] or $\underline{c}d^9:d^8\underline{L}$[34] states. Therefore, peak B intensity appears to be greatly enhanced at the surface of such nanostructured NiO samples, as reported in the literature for similar systems.[39,40] The dependence of the signals on the take-off angle for Ni 2p and O 1s is discussed in the SI.

The Ni $2p_{3/2}$ XP spectrum of the NiO0.5 sample is reported in Figure 8b. In this case, a somewhat different line shape is detected for this ionization region when compared to the previous case. The double peak at low BE originating from contributions A and B in the reference sample is here broadened, with no possibility of discerning two separated components, and with its intensity maximum slightly shifted to higher BE values. Furthermore, the feature at ~862 eV (peak D in reference NiO spectrum) appears further broadened and with a shallower separation from the lower BE main peak. The simulation of such spectrum with the set of fitting parameters adopted for the reference sample was not successful, since it hardly reproduced the experimental signal, especially in the region between peaks A and B and on both high- and low-energy tails of the peak at 862 eV.

Taking into account the preparation conditions of NiO0.5 sample, in which the anodic polarization of NiO was carried out in a neutral aqueous solution, the possible presence of oxyhydroxide species with Ni ions displaying oxidation states >2 had to be considered.

Nickel oxyhydroxide presents two polymorphs, β- and γ-NiOOH, in which different ratios of mixed oxidation states for nickel atoms are present. It has been reported for the β-polymorph that nickel is present with an oxidation state close to +3[60] or slightly lower, due to the presence of small amounts of $Ni(OH)_2$.[61−63] The γ- polymorph, instead, presents nickel with oxidation state of 3.5–3.7,[60] and a stoichiometry $0.835NiO_2{\cdot}0.165Ni(OH)_2$.[61] According to such data, the

dx.doi.org/10.1021/am403671h | ACS Appl. Mater. Interfaces 2014, 6, 143−152

simulation of Ni 2p XP spectrum of NiO0.5 sample has been here performed using a fitting data set containing the Gupta–Sen (GS) multiplets and shake-up-related satellites calculated for a Ni^{3+} free ion[45,46] and previously applied to bulk NiOOH with success.[44] The relative positions of the seven GS components here considered (these have been numbered 1–7 in the order of increasing BE) have been taken from ref 44 and have been reported in Table 3 together with the corresponding FWHM values. The results show that a satisfactory reconstruction of experimental signal could be obtained, suggesting that oxidation of native NiO at 0.5 V in H_2O/KCl at pH = 7.2 leads to the formation of a surface layer (or islands) of β-NiOOH, compatible with already reported electrochemical results.[60,64] Nevertheless, we cannot rule out the presence of residual Ni(II) species, which might be tightly associated to the β-NiOOH phase.[65] A fitting procedure accounting for both +3 and +2 oxidation states based on a fourteen-components double GS multiplet sets[44] was not attempted, due to the difficulty in managing with such a high number of unresolved peaks and with the risk of losing control on chemical information.

In spectrum c of Figure 8, the Ni 2p XP region of NiO0.85 sample is reported. In this sample a polarization at 0.85 V, above the second oxidation peak displayed in the CV trace, was applied. The simulation of Ni 2p XP spectrum was performed maintaining the fitting parameter set of the untreated NiO sample, the significant difference between these two spectra residing in the relative intensities of peaks B and A. In fact, the NiO0.85 sample displays a higher B/A area ratio (1.58) compared to reference NiO sample (1.45). High voltage oxidation (in proximity of O_2 evolution) of nickel compounds in alkaline aqueous electrolytes yields highly oxidized nickel species, such as Ni^{4+}.[66] It has been reported that the oxidation of NiO to γ-NiOOH brings about a fractional Ni oxidation state of 3.5–3.7,[60] due to the co-presence of different phases with a fractional composition $0.835NiO_2 \cdot 0.165Ni(OH)_2$,[61] in which nickel is actually present as a Ni^{4+} and Ni^{2+} species. Another compound where Ni^{4+} is present is the peroxide $NiOO_2$, which was proposed as an intermediate species in the process of the electrocatalytic formation of O_2.[67] This attribution is nevertheless controversial, since ex situ XPS[44] and in situ X-ray absorption fine structure spectroscopy (XANES)[68] studies on γ-NiOOH did not show the presence of Ni^{4+} species. This was confirmed by another combined study with near normal incidence reflectance spectroelectrochemistry (NNIRS) and cyclic voltammetry.[69,70] Some authors were recently able to characterize with XANES and EXAFS spectroscopy the compound $K_2Ni(H_2IO_6)_2$ (potassium nickel(IV) paraperiodate), in which solely Ni^{4+} is present.[71] They succeeded in establishing a correlation between spectroscopic features and oxidation state of nickel oxyhydroxides, confirming the predominance of Ni^{4+} centers in the γ-NiOOH phase. In the same study the authors could identify the transformation of β-NiOOH into γ-NiOOH upon anodization of a Ni-based catalyst at 1.0 V vs NHE,[71] which closely matches the second peak of oxidation at 0.75 V vs Ag/AgCl of our sample (Figure 2).

In the fitting procedure of our oxidized sample, we have used the same data set of peaks applied to untreated NiO. In fact, γ-NiOOH has a layered structure made of sheets of edge-sharing NiO_6 octahedra intercalated by water molecules or alkali ions,[72] whose formation on a NiO substrate might induce significant distortion and mismatch between the two phases. Except for the calculated multiplet envelopes by Gupta and Sen,[46] only one example of a low-resolution Ni 2p XP spectrum of a pure Ni^{4+} compound has been reported in the literature.[73] In our case, we report the first-to-date XP spectrum of what we propose to be an electrochemically generated very thin layer of a mixed valence Ni oxide with a predominant +4 oxidation state. Its XPS fingerprint in the Ni 2p region would be similar to that of NiO, with the difference of an apparently giant *surface* and nonlocal screening effect, likely due to a breakdown of bulk NiO tridimensional symmetry and transformation into a layered highly swollen structure, which greatly enhances the intensity of peak B at 855.6 eV.

O 1s. In Figure 9, the series of O 1s XP spectra of samples (a) NiO, (b) NiO0.5, and (c) NiO0.85 is reported, with corresponding BE positions, FWHM values, and chemical assignment summarized in Table 4. The spectrum of reference NiO sample shows the typical doubly peaked feature, where peak A′ falls at 529.4 eV and peak B′ at 531.3 eV. Peak A′ is

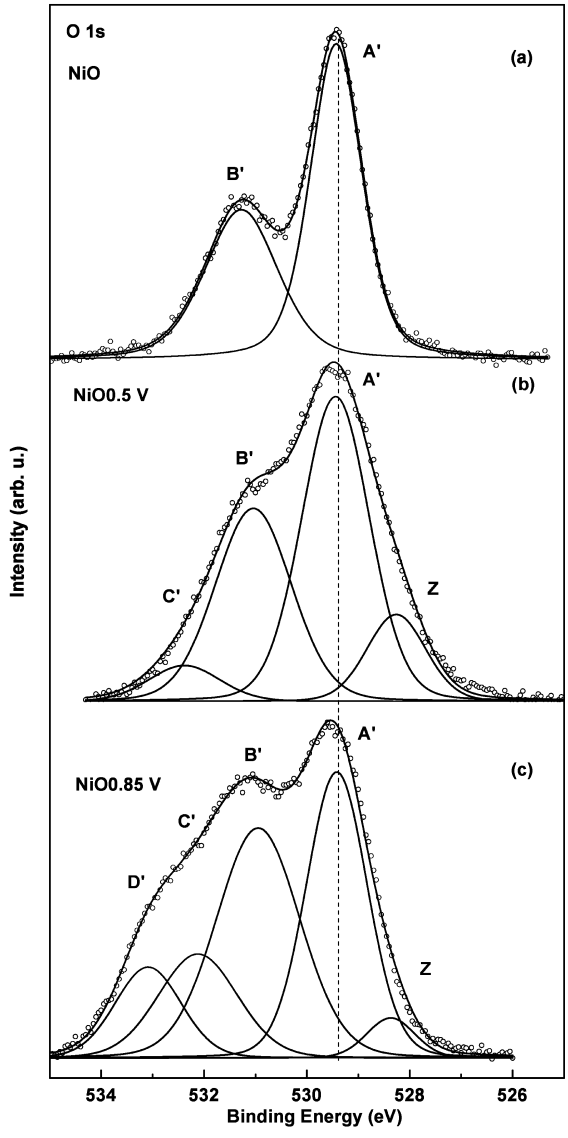

Figure 9. O 1s XP experimental (dots) spectra of (a) NiO, (b) NiO0.5, and (c) NiO0.85 samples recorded at take-off angle θ = 83° with Mg Kα X-ray source and fitting reconstruction (line) with single components marked as A′, B′, C′, D′, and Z.

dx.doi.org/10.1021/am403671h | ACS Appl. Mater. Interfaces 2014, 6, 143–152

Table 4. Binding Energies (eV)/FWHM (eV) Values of Peaks (with Associated Assignment) Used in the Fitting of the O 1s Spectra[a]

	peak A′	peak B′	peak C′	peak D′	peak Z
sample	NiO	$Ni(OH)_2$	$H_2PO_4^-/HPO_4^{2-}$	H_2O	O^{2-}–Na^+
NiO	529.4/1.19	531.3/1.68			
NiO0.5	529.4/1.55	531.0/1.75	532.4/1.63		528.3/1.60
NiO0.85	529.4/1.40	530.9/1.80	532.1/1.81	533.1/1.51	528.4/1.10

[a]Spectra were acquired using Mg Kα photons at θ = 83° take-off angle.

attributed to bulk O^{2-} ligands in the NiO_6 octahedron with the full complement of nearest neighbor atoms and is thus associated to bulk NiO.[74] Peak B′ has been associated in the past to the presence of chemisorbed OH species, which naturally form on the surface of NiO upon exposure to atmospheric conditions.[28] The same authors demonstrated that in a freshly cleaved NiO (100) single crystal such peak is not present and neither it is formed upon repeated Ar^+ ion sputtering cycles. Other authors reported that Li-doped NiO does show a high BE satellite in the O 1s region, explaining it as a result of O_2^{2-} defect structures formed at grain boundaries upon preparation of the oxide in dry O_2 atmosphere.[22] Such signal tends to disappear upon electron bombardment, which restores O^{2-} ions at the surface. Furthermore, in NiO this O 1s feature neither is related to hole doping through Li ions insertion,[22] nor to neighboring coordination and layer thickness.[23] The insensitivity of O 1s XPS signal to the presence of holes residing in the O 2p band was demonstrated with calculations on Cu_2O_7 clusters.[75] With these premises, we attribute the feature B′ in our spectra to surface hydroxyl groups bound to Ni atoms of the NiO network.

Upon polarization at 0.5 V in a aqueous $KCl/H_2PO_4^-/HPO_4^{2-}$ solution (sample NiO0.5, spectrum b of Figure 9) a broader signal has been detected and simulated with four components. The first peak (A′) has the same assignment of that in the NiO sample, with the only difference of a larger FWHM, and is also found in the spectrum of sample NiO0.85 with comparable FWHM. Also the second peak (B′) at 531.1 eV is attributed to the −OH termination of the NiO surface. Additional peaks are needed in this case to reproduce the experimental trace of XP spectrum of NiO0.5 sample. In fact, a third peak (C′) has been introduced at 532.4 eV and associated to adventitious residuals of $H_2PO_4^-$ and HPO_4^{2-} ions from the buffering agent of the electrolyte solution. In these anions oxygen atoms are bound to phosphorus in the +5 oxidation state. The BE position of such component is in agreement with literature data.[76]

A fourth peak (Z) was also needed to obtain a satisfactory simulation of the experimental spectrum. Such a peak, falling at 528.3 eV, i.e. a lower BE value than that of peak A′ in NiO, is here hypothesized to be due to oxygen anions interacting with alkali ions. In fact, such a very low BE for O 1s signal has only been reported for alkaline and alkaline-earth oxides.[74] In our case, the proposed formation of a thin films of β-NiOOH species at the surface of NiO nanostructures upon anodization at E = 0.5 V may call for the presence of alkali ions possibly intercalated in the layered oxyhydroxide structures. Signals from Na^+ ions coming from the buffering agent have indeed been detected in our samples after polarization both at 0.5 and 0.85 V (not shown).

Spectrum c of Figure 9 shows the O 1s region of NiO0.85 sample. In order to simulate the experimental signal, the same peaks as in NiO0.5 sample were utilized, with the exception of one more contribution added at high BE. Such an additional component at 533.1 eV is attributed to adsorbed water,[74] which may come from both the electrolyte and the atmosphere. The increased amount of incorporated water in NiO0.85 sample with respect to NiO0.5, as detected by O 1s signal, is coherent with the higher hydration level achieved during the formation of the γ-NiOOH phase, which can include water molecules in its layered structure.[71,72,77]

CONCLUSIONS

We have prepared nanoporous NiO electrodes by applying a technique based on the sinterization of NiO nanoparticles (diameter ≈50 nm) sprayed onto FTO glass. The sintering step involves heating from a plasma-assisted microwave source and already proved successful in the preparation of efficient nanostructured NiO coatings in the configuration of thin films ($0.2 < l < 3.5$ μm) for solar energy conversion purposes. The prepared nanoporous NiO electrodes have been characterized with cyclic voltammetry, which has shown the occurrence of two reversible surface-confined oxidation events associated to the change in oxidation state of Ni centres from Ni(II) to Ni(III) and from Ni(III) to Ni(IV). The effects of polarization of NiO nanoporous thin films at oxidative potential corresponding to the completion of the two oxidation reactions was investigated with XPS. This technique was used in the most surface-sensitive configuration allowed by the experimental setup in order to investigate the nature of chemical species formed upon polarization at oxidative potentials. The study of Ni 2p ionization and the electronic relaxation phenomena thereto associated, together with the findings on the O 1s region and the Auger parameter, confirmed the hypothesis of the sequential formation of β- and γ-NiOOH species and, in the latter case, showed for the first time the XPS features of an electrochemically generated Ni(IV) species. The changes of nickel oxidation state introduced electrochemically in the surface of nanoporous NiO in contact with water, together with the evidence of superficial nickel having a valence higher than +2/+3, can be involved in the cathodic mechanisms of water splitting and, eventually, in the coloration processes of electrochromic NiO in aqueous electrolytes. Furthermore, since the same changes in Ni oxidation state may occur when a water-contaminated organic electrolyte is used for cathodic DSCs, we consider the "limit" condition of the use of a pure aqueous electrolyte in this study as the starting point to further investigating the role of water, as an impurity in organic technical electrolytes, on the kinetics of charge photoinjection and hole transport of cathodic DSCs based on NiO photoactive electrodes prepared with our advanced method of sintering. In doing so, the ex-situ spectroelectrochemical procedure here presented could be successfully exploited for the evaluation of sensitized nanoporous NiO electrodes before and after operation in devices of interest, like p-type DSCs, for the

quality check of the preparation procedure and as test of performance loss.

■ ASSOCIATED CONTENT

Supporting Information

Cyclic voltammograms and chronoamperometric curves of NiO sample polarized at two different potentials (thickness: 2.5 μm). Linear dependence of the 2nd anodic peak with scan rate for a NiO sample with thickness of 0.2 μm. Further XPS material, comprising depth of analysis data and discussions on Auger parameter and surface sensitivity. This material is available free of charge via the Internet at http://pubs.acs.org.

■ AUTHOR INFORMATION

Corresponding Author

*E-mail: andrea.marrani@uniroma1.it. Phone: +39 0649913344. Fax: +39 06490324.

Notes

The authors declare no competing financial interest.

■ ACKNOWLEDGMENTS

D.D. acknowledges the financial support from the University of Rome "LA SAPIENZA" through the program Ateneo 2012 (Protocol No. C26A124AXX).

■ REFERENCES

(1) Passerini, S.; Scrosati, B. *J. Electrochem. Soc.* **1994**, *141*, 889−895.
(2) Granqvist, C. G. *Sol. Energ. Mat. Sol. C.* **2007**, *91*, 1529−1598.
(3) Lang, J. W.; Kong, L. B.; Liu, M.; Luo, Y. C.; Kang, L. *J. Solid State Electr.* **2010**, *14*, 1533−1539.
(4) Svegl, F.; Surca Vuk, A.; Hajzeri, M.; Slemenik Perse, L.; Orel, B. *Sol. Energy Mater. Sol. C.* **2012**, *99*, 14−25.
(5) Gillaspie, D.; Norman, A.; Tracy, C. E.; Pitts, J. R.; Lee, S. H.; Dillon, A. *J. Electrochem. Soc.* **2010**, *157*, H328−H331.
(6) Irwin, M. D.; Buchholz, D. B.; Hains, A. W.; Chang, R. P. H.; Marks, T. J. *Proc. Natl. Acad. Sci. U.S.A.* **2008**, *105*, 2783−2787.
(7) Awais, M.; Rahman, M.; MacElroy, J. M. D.; Dini, D.; Vos, J. G.; Dowling, D. P. *Surf. Coat. Tech.* **2011**, *205*, S245−S249.
(8) Qin, P.; Zhu, H.; Edvinsson, T.; Boschloo, G.; Hagfeldt, A.; Sun, L. *J. Am. Chem. Soc.* **2008**, *130*, 8570−8571.
(9) Gibson, E. A.; Amanda, L. S.; Le Pleux, L.; Fortage, J.; Boschloo, G.; Blart, E.; Pellegrin, Y.; Odobel, F.; Hagfeldt, A.; Hammarström, L. *Angew. Chem. Int. Ed.* **2009**, *48*, 4402−4405.
(10) Li, L.; Gibson, E. A.; Qin, P.; Boschloo, G.; Gorlov, M.; Hagfeldt, A.; Sun, L. *Adv. Mater.* **2010**, *22*, 1759−1762.
(11) Li, L.; Duan, L.; Wen, F.; Li, C.; Wang, M.; Hagfeldt, A.; Sun, L. *Chem. Commun.* **2012**, *48*, 988−990.
(12) Tong, L.; Iwase, A.; Nattestad, A.; Bach, U.; Weidelener, M.; Götz, G.; Mishra, A.; Bäuerle, P.; Amal, R.; Wallace, G.G.; Mozer, A.J. *Energy Environ. Sci* **2012**, *5*, 9472−9475.
(13) see for example the reviews: Hüfner, S. *Adv. Phys.* **1994**, *43*, 183−356. Hagelin-Weaver, H. A. E.; Weaver, J. F.; Hoflunda, G. B.; Salaita, G. N. *J. Electron Spectrosc. Relat. Phenom.* **2004**, *134*, 139−171.
(14) Zaanen, J.; Sawatzky, G. A.; Allen, J. W. *Phys. Rev. Lett.* **1985**, *55*, 418−421.
(15) Sawatzky, G. A.; Allen, J. W. *Phys. Rev. Lett.* **1984**, *53*, 2339−2342.
(16) Hüfner, S. *Solid State Commun.* **1985**, *53*, 707−710.
(17) Biesinger, M. C.; Lau, L. W. M.; Gerson, A. R.; Smart, R. St. C. *Phys. Chem. Chem. Phys.* **2012**, *14*, 2434−2442.
(18) Fujimori, A.; Minami, F.; Sugano, S. *Phys. Rev. B* **1984**, *29*, 5225−5227.
(19) Fujimori, A.; Minami, F. *Phys. Rev. B* **1984**, *30*, 957−971.
(20) Hüfner, S. *Solid State Commun.* **1984**, *52*, 793−796.
(21) Bredow, T.; Gerson, A. R. *Phys. Rev. B* **2000**, *61*, 5194−5201.
(22) Van Elp, J.; Eskes, H.; Kuiper, P.; Sawatzky, G. A. *Phys. Rev. B* **1992**, *45*, 1612−1622.
(23) Alders, D.; Voogt, F.C.; Hibma, T.; Sawatzky, G. A. *Phys. Rev. B* **1996**, *54*, 7716−7719.
(24) Tyuliev, G.; Sokolova, M. *Appl. Surf. Sci.* **1991**, *52*, 343−349.
(25) Payne, B. P.; Biesinger, M. C.; McIntyre, N. S. *J. Electron Spectr. Relat. Phenom.* **2009**, *175*, 55−65.
(26) Roberts, M. W.; Smart, R.; St, C. *J. Chem Soc., Faraday Trans. 1* **1984**, *80*, 2957−2968.
(27) Tomellini, M. *J. Chem Soc., Faraday Trans. 1* **1988**, *84*, 3501−3510.
(28) Uhlenbrock, S.; Scharfschwerdt, C.; Neumann, M.; Illing, G.; Freund, H.-J. *J. Phys.: Condens. Matter* **1992**, *4*, 7973−7978.
(29) Kim, K. S.; Winograd, N. *Surf. Sci.* **1974**, *43*, 625−643.
(30) Langell, M. A. *Surf. Sci.* **1987**, *186*, 323−338.
(31) Oku, M.; Tokuda, H.; Hirokawa, K. *J. Electron Spectr. Relat. Phenom.* **1991**, *53*, 201−211.
(32) Tomellini, M. *J. Electron Spectr. Relat. Phenom.* **1992**, *58*, 75−78.
(33) Kuiper, P.; Kruizinga, G.; Ghijsen, J.; Sawatzky, G. A.; Verweij, H. *Phys. Rev. B* **1989**, *62*, 221−224.
(34) Van Veenendaal, M. A.; Sawatzky, G. A. *Phys. Rev. Lett.* **1993**, *70*, 2459−2462.
(35) Oku, M.; Hirokawa, K. *J. Electron Spectr. Relat. Phenom.* **1977**, *10*, 103−110.
(36) Altieri, S.; Tjeng, L. H.; Tanaka, A.; Sawatzky, G. A. *Phys. Rev. B* **2000**, *61*, 13403−13409.
(37) Atanasov, M.; Reinen, D. *J. Electron Spectr. Relat. Phenom.* **1997**, *86*, 185−199.
(38) Soriano, L.; Preda, I.; Gutiérrez, A.; Palacín, S.; Abbate, M.; Vollmer, A. *Phys. Rev. B* **2007**, *75*, 233417.
(39) Preda, I.; Mossanek, R. J. O.; Abbate, M.; Alvarez, L.; Méndez, J.; Gutiérrez, A.; Soriano, L. *Surf. Sci.* **2012**, *606*, 1426−1430.
(40) Biju, V.; Abdul Khadar, M. *J. Nanopart. Res.* **2002**, *4*, 247−253.
(41) Peck, M. A.; Langell, M. A. *Chem. Mater.* **2012**, *24*, 4483−4490.
(42) D'Addato, S.; Grillo, V.; Altieri, S.; Tondi, R.; Valeri, S.; Frabboni, S. *J. Phys.: Condens. Matter* **2011**, *23*, 175003.
(43) Mossanek, R. J. O.; Preda, I.; Abbate, M.; Rubio-Zuazo, J.; Castro, G. R.; Vollmer, A.; Gutiérrez, A.; Soriano, L. *Chem. Phys. Lett.* **2011**, *501*, 437−441.
(44) Grosvenor, A. P.; Biesinger, M. C.; Smart, R.; St, C.; McIntrye, N. S. *Surf. Sci.* **2006**, *600*, 1771−1779.
(45) Gupta, R. P.; Sen, S. K. *Phys. Rev. B* **1974**, *10*, 71−77.
(46) Gupta, R. P.; Sen, S. K. *Phys. Rev. B* **1975**, *12*, 15−19.
(47) Gibson, E. A.; Awais, M.; Dini, D.; Dowling, D. P.; Pryce, M.T.; Vos, J. G.; Boschloo, G.; Hagfeldt, A. *Phys. Chem. Chem. Phys.* **2013**, *15*, 2411−2420.
(48) Awais, M.; Dowling, D.P.; Rahman, M.; Vos, J.G.; Decker, F.; Dini, D. *J. Appl. Electrochem.* **2013**, *43*, 191−197.
(49) McConnell, M. L.; Dowling, D. P.; Pope, C.; Donnelly, K.; Ryder, A. G.; O'Connor, G. M. *Diam. Relat. Mater.* **2002**, *11*, 1036−1040.
(50) Biesinger, M. C.; Payne, B. P.; Lau, L. W. M.; Gerson, A.; Smart, R.; St, C. *Surf. Interface Anal.* **2009**, *41*, 324−332.
(51) Powell, C. J.; Jablonski, A. *NIST Electron Inelastic-Mean-Free-Path Database*, Version 1.2, SRD 71; National Institute of Standards and Technology: Gaithersburg, MD, 2010.
(52) Tanuma, S.; Powell, C. J.; Penn, D. R. *Surf. Interface Anal.* **1991**, *17*, 927−939.
(53) Bode, H.; Dehmelt, K.; Witte, J. *Electrochim. Acta* **1966**, *11*, 1079−1087.
(54) Lyons, M. E. G.; Brandon, M. P. *Int. J. Electrochem. Sc.* **2008**, *3*, 1386−1424.
(55) Boschloo, G.; Hagfeldt, A. *J. Phys. Chem. B* **2001**, *105*, 3039−3044.
(56) Yohe, D.; Riga, A.; Greef, R.; Yeager, E. *Electrochim. Acta* **1968**, *13*, 1351−1358.
(57) Tench, D. M.; Yeager, E. *J. Electrochem. Soc.* **1973**, *120*, 164−171.

(58) Awais, M.; Dini, D.; Don MacElroy, J. M.; Halpin, Y.; Vos, J. G.; Dowling, D.P. *J. Electroanal. Chem.* **2013**, *689*, 185−192.
(59) Dini, D.; Decker, F. *Electrochim. Acta* **1998**, *43*, 2919−2923.
(60) Wherens-Dijksma, M.; Notten, P. H. L. *Electrochim. Acta* **2006**, *51*, 3609−3621.
(61) Beverskog, B.; Puigdomenech, I. *Corros. Sci.* **1997**, *39*, 969−980.
(62) Barnard, R.; Randell, C. F.; Tye, F. L. *J. Appl. Electrochem.* **1980**, *10*, 109−125.
(63) Barnard, R.; Randell, C. F. *J. Appl. Electrochem.* **1983**, *13*, 27−38.
(64) Ratcliff, E. L.; Meyer, J.; Steirer, K. X.; Garcia, A.; Berry, J. J.; Ginley, D. S.; Olson, D. C.; Kahn, A.; Armstrong, N. R. *Chem. Mater.* **2011**, *23*, 4988−5000.
(65) Actually, the relative intensities of the GS peaks here used in the simulation of NiO0.5 spectrum are not equal to those calculated in ref 46 for a Ni^{3+} free ion. Such a difference might call for a possible co-presence of Ni^{2+} species.
(66) Desilvestro, J.; Corrigan, D. A.; Weaver, M. J. *J. Electrochem. Soc.* **1988**, *135*, 885−892.
(67) Juodkazis, K.; Juodkazyte, J.; Vilkauskaite, R.; Jasulaitiene, V. *J. Solid State Electrochem.* **2008**, *12*, 1469−1479.
(68) Hu, Y. N.; Bae, I. T.; Mo, Y. B.; Antonio, M. R.; Scherson, D. A. *Can. J. Chem.* **1997**, *75*, 1721−1729.
(69) Yeo, B. S.; Bell, A. T. *J. Phys. Chem. C* **2012**, *116*, 8394−8400.
(70) Zhang, C. J.; Park, S. M. *J. Electrochem. Soc.* **1989**, *136*, 3333−3342.
(71) Bediako, D. K.; Lassalle-Kaiser, B.; Surendranath, Y.; Yano, J.; Yachandra, V. K.; Nocera, D. G. *J. Am. Chem. Soc.* **2012**, *134*, 6801−6809.
(72) Yang, X.; Takada, K.; Itose, M.; Ebina, Y.; Ma, R.; Fukuda, K.; Sasaki, T. *Chem. Mater.* **2008**, *20*, 479−485.
(73) Yamashita, M.; Ito, T. *Inorg. Chim. Acta* **1984**, *87*, LS−L7.
(74) Dupin, J.-C.; Gonbeau, D.; Vinatier, P.; Levasseur, A. *Phys. Chem. Chem. Phys.* **2000**, *2*, 1319−1324.
(75) Eskes, H.; Sawatzky, G. A. *Phys. Rev. B* **1991**, *43*, 119−129.
(76) Landis, W. J.; Martin, J. R. *J. Vac. Sci. Technol. A* **1984**, *2*, 1108−1111.
(77) Oliva, P.; Leonardi, J.; Laurent, J. F. *J. Power Sources* **1982**, *8*, 229−255.